The International Journal of Advanced Manufacturing Technology
https://doi.org/10.1007/s00170-026-17865-5

ORIGINAL ARTICLE

A geometry-based predictive framework for charge welds: a tool for extrusion scrap reduction and die design optimization

Riccardo Pelaccia[1] · Marco Negozio[2] · Adrian H. A. Lutey[2] · Sara Di Donato[3] · Tommaso Pinter[4] · Lorenzo Donati[3] · Barbara Reggiani[1,5]

Received: 14 January 2026 / Accepted: 9 March 2026

Abstract
An innovative analytical model for predicting charge weld length in continuous extrusion is presented, with the goal of minimizing scrap and ensuring the structural performance of extruded profiles. By relying only on die and profile geometry, the approach offers major advantages over computationally expensive FEM simulations and experimental methods in terms of time and resources, while improving prediction accuracy compared with previous analytical formulations. The model covers a wider range of extrusion conditions and is applicable to complex industrially relevant profiles. In addition to parameters considered in earlier models, such as die volume, exit area and number of ports, the proposed method accounts for inlet area, feeding chamber area and angle, port area, exit area and profile wall thickness, providing a more complete description of material flow. A dataset from 12 experimentally analyzed extruded profiles was first acquired, then expanded through FEM simulations of 84 additional cases. Model coefficients were obtained via multivariate regression, achieving a mean absolute percentage error below 9%, significantly lower than previous analytical approaches. Based solely on geometric descriptors available early in the design stage, the model offers a fast and reliable tool for reducing charge weld length and supporting geometry-driven die development.

Keywords Extrusion process · Scrap optimization · Charge weld modeling · Process sustainability · Die design

1 Introduction

Low roughness, narrow dimensional tolerances and consistent mechanical strength along the entire profile are essential in hot extrusion of aluminum [1, 2], especially for structural applications where defects can cause in-service failure [3–6]. Charge welds are unavoidable defects in continuous extrusion caused by the introduction of new billets, where new material coated with oxides, dust and lubricant comes into contact with hot material remaining in the die from the previously extruded billet. With application of pressure and heat, the two regions form a fully bonded contact, creating a transition zone of mixed old and new material (Fig. 1), or charge weld, characterized by high levels of contaminants and low strength. This zone exhibits a parabolic shape within longitudinal sections, while it appears as a closed loop in transverse sections. Charge welds must be scrapped due to their inferior mechanical properties compared to the rest of the extruded profile.

Charge welds, also referred to as transverse welds in the literature, have been thoroughly examined in fundamental studies investigating aluminum extrusion. Saha [7] presented a systematic classification of defect types in industrial profiles, including weld seams generated at billet transitions. Valberg [8] instead presented an analysis of extrusion welding mechanisms, showing how local pressure, strain and surface conditions govern the formation and integrity of

✉ Marco Negozio
marco.negozio@unipr.it

1 Dipartimento di Scienze e Metodi dell'Ingegneria (DISMI), University of Modena and Reggio Emilia, Via Amendola 2, 42122 Reggio Emilia, Italy

2 Dipartimento di Ingegneria dei Sistemi e delle Tecnologie Industriali (DISTI), Università degli Studi di Parma, Parco Area delle Scienze, 181/A, Parma 43124, Italy

3 Dipartimento di Ingegneria Industriale (DIN), Università di Bologna, Viale Risorgimento 2, Bologna 40136, Italy

4 Almax Mori Srl, Via Matteotti 13, Mori 38065, Italy

5 InterMech - MO.RE, University of Modena and Reggio Emilia, Piazzale Europa 1, Reggio Emilia 42124, Italy

Published online: 16 March 2026

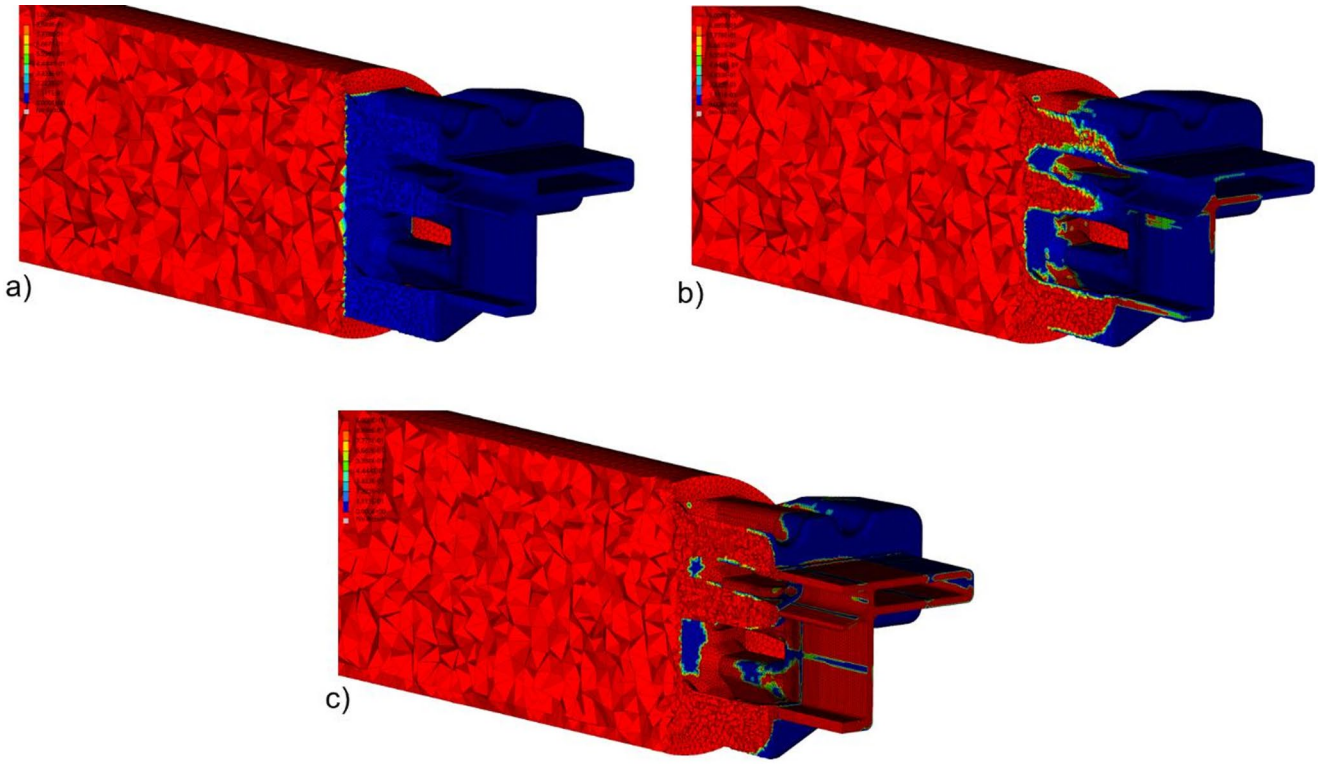

Fig. 1 Stages of billet material replacement during extrusion (red = new billet, blue = previous billet). **a**) Beginning of extrusion with the new billet; **b**) flow of new billet material through die to reach profile; **c**) profile almost entirely made up of new billet material

weld regions. Numerous subsequent studies have examined specific material responses based on experiments. Loukus et al. [9] reported reductions in strength associated with fragmented oxide films and heterogeneous recrystallization at the weld interface in AA6082-T4. Zhang et al. [10] analyzed oxide dispersion in porthole die weld seams in AA6061, demonstrating that redistribution and accumulation of surface oxides has a significant impact on bonding quality and microstructural continuity. Den Bakker et al. [11] performed microstructural analysis and mechanical characterization of AA6082 extruded profiles, demonstrating how gradients in grain morphology and hardness arise from thermal deformation during billet transition. Lou et al. [12] investigated AA6061 extruded profiles, identifying characteristic texture changes within the weld region associated with reduced tensile strength. Yu et al. [13] instead compared longitudinal and transverse welds, demonstrating that impurity concentration and interface morphology strongly affect corrosion resistance and overall structural integrity.

While early studies primarily focused on the microstructural features and mechanical behavior within charge welds, subsequent investigations examined how process parameters influenced their formation, extent and the amount of scrap generated. Bingöl and Keskin [14] performed a series of experiments with AA6063 while varying extrusion speed and temperature, demonstrating that higher temperatures and lower speeds generally reduce weld severity and size. Zhang et al. [15] analyzed the transverse characteristics of charge welds in AA7N01 hollow profiles, demonstrating that weld morphology depends strongly on material flow and die design. Qamar et al. [16] instead investigated the influence of profile shape complexity, identifying geometric features that exacerbate weld defects. Oberhausen et al. [17] focused on scrap reduction strategies, showing that optimization of billet handling and process control can significantly decrease the quantity of discarded material. More recently, Sariyarlioglu et al. [18] investigated the mechanisms of charge weld evolution, combining process monitoring with metallurgical analysis to identify the main parameters governing weld formation.

Recently, increasing focus has been placed on the use of numerical simulations to study charge weld formation due to the ease and flexibility with which the effects of process parameters and die geometry can be investigated. Li et al. [19], den Bakker et al. [20] and Reggiani et al. [21] employed conventional FEM simulations to model transverse weld formation, analyzing the influence of billet flow and die geometry on weld morphology. Mahmoodkhani et al. [22, 23] extended these simulations to billet-on-billet extrusion, demonstrating the role of material flow patterns on weld development. Pinter et al. and Negozio et al. [24, 25] applied FEM simulations to both front-end and back-end

defects, validating their predictions against experimental data while studying the effects of process and geometric parameters on weld behavior. More recently, Di Donato et al. [26, 27] employed phase-field and Cahn-Hilliard models to simulate the interaction between new and old billet materials, achieving close alignment with experimental outcomes. Pelaccia et al. [28] instead compared the results of different FEM models for the extrusion of hollow profiles, analyzing thermal fields, profile speed, defect evolution and microstructure. Sariyarlioglu et al. [29] combined experiments and numerical modeling to investigate charge weld evolution in hollow aluminum extruded profiles, providing comprehensive validation of simulation outcomes.

Various studies have been performed with the aim of directly correlating the effects of die geometry with the extent of charge welds. Pinter et al. investigated the impact of port volume by considering dies with two, three and four legs, demonstrating that greatest defect length occurs in a two-leg configuration due to the larger port volume and therefore larger amount of old billet material that must be replaced by new material [24]. In a subsequent study, Pinter et al. [30] examined the influence of port shape convergence on charge weld formation for a complex industrial profile, finding that convergent die geometry leads to shorter charge welds due to dynamic compression of the material, minimizing dead-metal flow. Zhang et al. [31] investigated charge weld evolution within a hollow profile for high-speed train applications, both experimentally and numerically, observing faster appearance of welding defects in thicker regions of the profile. Mahmoudkhani et al. [23] compared cylindrical and convergent port shapes, demonstrating that charge weld formation is strongly affected by port geometry beyond simple volumetric considerations. Crosio et al. [32] showed that reducing the size of the port inlet is a decisive factor in decreasing material scrap associated with charge welds. Finally, Qamar et al. [16, 33] correlated charge weld characteristics to several shape complexity indices based on geometric parameters such as the perimeter, area, weight per unit length, circumscribing circle diameter, minimum wall thickness, extrusion ratio and number of ports.

Experimental measurement of charge weld length involves locating the stop mark (a visible surface defect generated when the extrusion process is stopped to load a new billet) followed by cutting the profile, polishing and etching to detect the defect and measure its extent. Although accurate, this method takes hours or days, with potentially significant impacts on the effectiveness of process optimization. FEM analysis can instead predict the extent of charge welds for various die shapes and process parameters but requires detailed CAD models, extensive meshing and calculation times ranging from minutes to days depending on complexity, making the approach potentially impractical for industrial implementation. Only a limited number of analytical models have been proposed to predict and estimate the extent of charge weld defects in aluminum extrusion. Approaches by Valberg [8], Saha [34] and Jowett et al. [35] correlate the defect length to die and billet characteristics by accounting for various combinations of geometric parameters such as the thickness of the co-extruded layer, perimeter and length of the profile, volume of material in the die port and welding chamber, profile exit area and number of die openings. While these models are undoubtedly faster and less resource-intensive than experimental measurements or FEM simulations, they are nonetheless restricted in terms of accuracy and applicability, resulting in limited uptake in industrial settings.

An innovative analytical model for charge weld prediction has therefore been developed within this work, providing a more complete representation of material flow and more accurate results over a wider range of conditions compared to previous approaches. Further to the geometric parameters considered by Valberg [8], Saha [34] and Jowett et al. [35], the present work accounts for the inlet area, the area feeding the welding chamber and the exit area, as well as the angle of the feeding chamber, port area and profile wall thickness, amongst other parameters. In order to calibrate coefficients within the model, a total of 12 extrusion experiments were performed by Almax-Mori to acquire an initial dataset. A FEM simulation was then developed in Altair HyperXtrude® and validated with experimental data by comparing the experimental and simulated profile exit temperatures and extrusion loads. Subsequently, an additional 84 extrusion simulations were performed to complete the dataset for calibration of the analytical model. Coefficients within the model were determined through multivariate regression in MATLAB, explicitly incorporating profile geometry and material parameters to maximize the predictive accuracy and ensure broad applicability across different extrusion scenarios. The model showed excellent agreement with measured charge weld lengths, outperforming existing analytical formulations, yielding a fast, reliable and easy-to-implement analytical tool for charge weld prediction without the need for extensive simulations to support both industrial practice and early-stage die design.

2 Materials and methods

2.1 Experimental investigation

Twelve industrial aluminum extrusion profiles, denoted Profile_exp_1 to Profile_exp_12, were selected for experiments. The range of geometric parameters addressed in experiments is summarized in Table 1, with profiles

Table 1 Die and profile geometric parameter ranges addressed in experiments

Die/Profile parameter	Min value	Max value
V [mm^3]	3.0×10^5	2.7×10^6
A [mm^2]	165.3	2776.0
n	1	4
dev	1	1.8235
dev_4	2.8350	39.1417
dev_5	1.3917	2.6439
R_1	0.6300	2.4736
R_2	2.2282	31.1111
C_{d_die}	1.3980	1.8305
C_3	8.3	146.9
L_1	1.7483	64.7165

comprising both solid and hollow profile sections with varying levels of geometric complexity representing typical commercial applications. Profiles were extruded from AA6060, AA6082 and AA6063 aluminum alloy billets, with each profile produced from a single alloy. The three investigated alloys are part of the 6XXX series, which accounts for the majority of industrial aluminum extrusion applications. Moreover, the selected materials include both alloys characterized by relatively low flow stress and high extrudability such as AA6060 and AA6063, typically classified as low-strength alloys, and AA6082, which is generally classified as a medium-strength alloy [36]. This combination allowed the dataset to capture a broad range of billet material flow stresses, ensuring representativeness across different extrudability conditions. Together with the comprehensive set of profiles and parameter ranges employed, this material selection enabled a robust evaluation of the influence of geometry on extrusion behaviour.

All profiles were initially cut into 100 mm samples, with regions in which charge welds were present cut into smaller sections to allow detailed investigation into evolution of the defect. All samples were polished on the advancing side relative to the extrusion direction with progressively finer abrasive paper up to P1200, followed by etching with a 30% sodium hydroxide solution in water at 60 °C for 45–90 s to reveal the microstructure. An example of the acquired microstructure is shown in Fig. 2. To assess and quantify the charge welds, each section was photographed to allow measurement of contours enclosing new billet material, with the percentage of new material determined as a function of the distance from the stop mark. The defect was considered to be extinct when 99% of the section was made up of new material. This threshold was slightly higher than the typical value of approximately 95% [29] to account for difficulties in evaluating material behavior as the new billet approaches the profile surface. Final values of charge weld length were stored within an initial dataset for validation of FEM simulations and later use for calibrating the developed analytical model.

2.2 FEM simulation

Numerical FEM simulations of all extruded profiles were performed using HyperXtrude® by Altair Engineering. The 3D CAD geometries of each tool were firstly processed through Boolean subtraction operations to define the material flow domains, allowing implementation of Arbitrary Lagrangian–Eulerian (ALE) transient simulations. The computational model included a detailed representation of the billet, feeder, porthole, pocket, bearing and profile

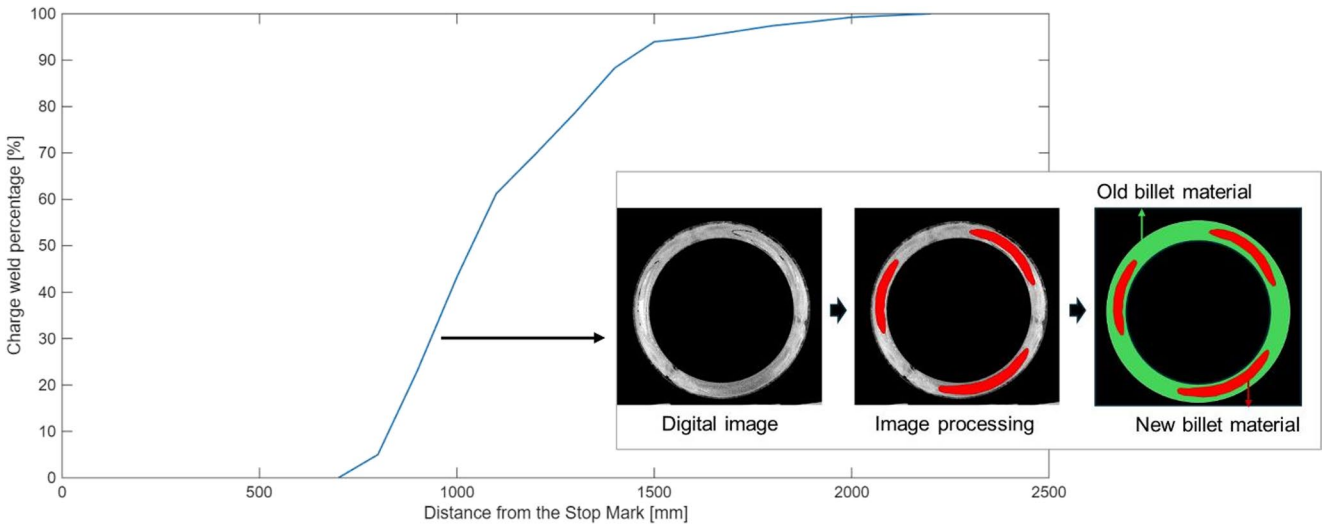

Fig. 2 Example of charge weld evolution as a function of distance from the stopmark based on metallographic analysis of material flow from the incoming billet. Red: new billet material; Green: old billet material

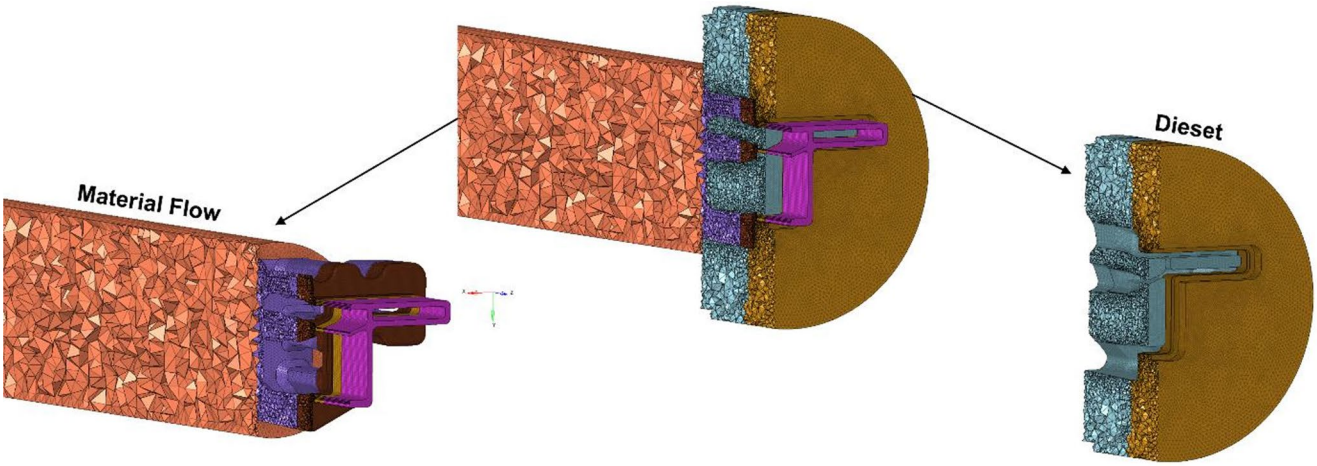

Fig. 3 Die mesh and material flow in HyperXtrude®

Table 2 Hensel-Spittel parameters employed within simulations for AA6082, AA6063 and AA6060 aluminum alloys

Hensel-Spittel parameters	AA6082	AA6063	AA6060
A [MPa]	568,000	1135.82	1014.7
m_1 [K^{-1}]	-0.002117	-0.004784	-0.00438
m_2	0.1059	0.077934	0.2425
m_3	0.08299	-0.225984	-0.0965
m_4	0.0009266	0.00197	-0.000438
m_5 [K^{-1}]	-0.0005221	-0.0003496	-0.000766
m_7	0.02343	0.008249	0.0939
m_8 [K^{-1}]	0.00006741	0.0004796	0.000291
m_9	-1.208	0	0

regions. The billet, feeder, porthole and pockets were discretized using 3D tetrahedral elements with four nodes each, while the bearing and profile regions were discretized with 3D prismatic elements with six nodes each to better capture the complex velocity and temperature gradients within these critical regions. Examples of meshing and material flow within HyperXtrude® are shown in Fig. 3.

All simulations adopted a viscoplastic friction model with a friction coefficient of 0.3 at the bearing interface and a sticking condition at the billet-container and billet-die interfaces. A convective heat transfer coefficient of 11,000 W/(m²·°C) was applied at the interfaces between the workpiece and tool [26]. At the die exit, a zero normal stress boundary condition was imposed to ensure realistic material outflow. The constitutive behavior of the aluminum alloys employed in experiments was described with the Hensel–Spittel model [37], where the flow stress, $\bar{\sigma}$, is a function of the strain, $\bar{\varepsilon}$, strain rate, $\dot{\bar{\varepsilon}}$, and temperature, T, as per Eq. (1). The corresponding coefficients, reported in Table 2, were taken from previous studies [38–40] for AA6082, AA6063 and AA6060 aluminum alloys. All material parameters were retrieved from the standard Altair material database.

Table 3 Results of FEM convergence analysis

Mesh size and time-step setting	Maximum extrusion load	Extrusion temperature	Computational time
Coarse	19.1 MN	535 °C	22 h
Fine	17.5 MN	542 °C	38 h
Extremely fine	17.5 MN	542 °C	46 h

$$\bar{\sigma} = A \cdot e^{m_1 T} \cdot \bar{\varepsilon}^{-m_2} \cdot \dot{\bar{\varepsilon}}^{-m_3} \cdot e^{\frac{m_4}{\bar{\varepsilon}}} \cdot (1+\bar{\varepsilon})^{m_5 T} \cdot e^{m_7 \bar{\varepsilon}} \cdot \dot{\bar{\varepsilon}}^{m_8 T} \cdot T^{m_9} \quad (1)$$

All FEM analyses were performed as transient simulations with moving boundaries. With this approach, the bearing, porthole, welding chamber and profile region mesh remained fixed throughout the process, while the billet mesh was continuously deformed and compressed by the ram displacement. To improve the accuracy of the transient solution, simulations were executed with a variable number of time steps, which were refined during critical stages of material flow [41]. In order to determine the most suitable mesh size and time-step values, a convergence analysis was carried out on Profile_exp_1. Results of the analysis are reported in Table 3. Three configurations were tested, including coarse, fine and extremely fine settings. In each case, the predicted maximum extrusion load, extrusion temperature and simulation time were recorded. This procedure made it possible to identify the optimal balance between accuracy and computational efficiency, ensuring reliable results without unnecessary computational cost. The performed mesh and time-step sensitivity analysis showed that refining discretization from coarse to fine produced improvements in both the predicted extrusion load and temperature, with the maximum load decreasing from 19.1 MN to 17.5 MN and the temperature increasing from 535 °C to 542 °C. However, further refinement to an extremely fine setting did not lead to any additional changes in either quantity, which remained

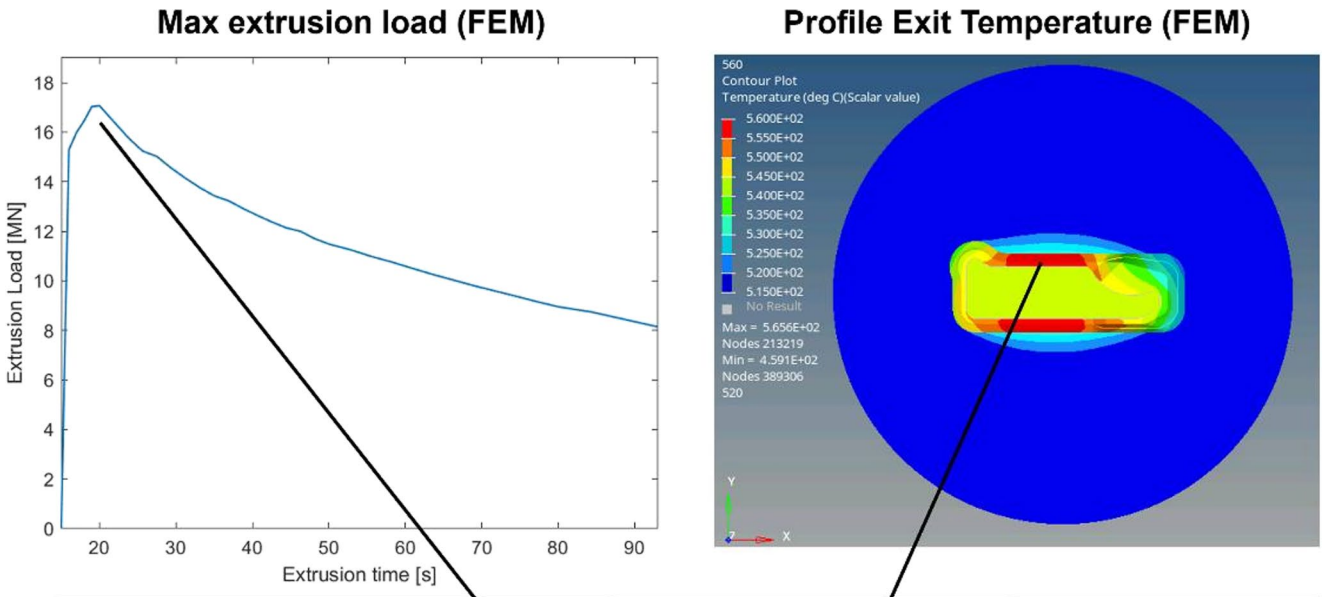

	Altair HyperXtrude	Experimental
Profile Exit Temperature [°C]	542 (**1.2% error**)	535 ±5
Max Extrusion Load [MN]	17.5 (**2.3% error**)	17.1 ±0.1

Fig. 4 Comparison between simulated and experimental profile exit temperature and max extrusion load for Profile_exp_1

Table 4 Die and profile geometric parameters ranges addressed in FEM simulations

Die/Profile parameter	Min Value	Max Value
V [mm^3]	5.9×10^5	3.4×10^7
A [mm^2]	225	1577
n	1	4
dev	1	7.1038
dev_4	1	25.8244
dev_5	1	10.5769
R_1	0.6300	13.2200
R_2	0.8325	32.1746
C_{d_die}	1.1785	1.7054
C_3	1	97.0852
L_1	2.6854	98.9295

identical to those obtained with the fine setting. The only effect of the extremely fine setting was a substantial increase in computational time, from 38 h to 46 h. The fine setting was therefore selected as the optimal balance between accuracy and computational cost.

Simulations were performed for the three different aluminum alloys employed in experiments, AA6060, AA6082 and AA6063, with Hensel–Spittel coefficients as reported in Table 2. The predicted extrusion loads and temperature distributions were validated against the 12 experimental cases. Differences between numerical predictions and experimental measurements of the extrusion load and profile exit temperature were consistently below 5%, confirming the robustness and accuracy of the proposed FEM model. An example of comparison between simulation and experimental results is provided in Fig. 4 for Profile_exp_1.

Once validation of the FEM model had been completed by comparing experimental and numerical data on extrusion load, profile exit temperature and charge weld extent (see Section 3.1), an additional 84 extruded profiles, denoted Profile_FEM_1 to Profile_FEM_84, were simulated to expand the original dataset. The range of geometric parameters addressed in the simulations is summarized in Table 4. The dataset includes profiles comprising both hollow and solid sections with varying levels of geometric complexity, covering a wider parameter range than the experimental cases and including both symmetric and asymmetric configurations representative of industrial die designs.

2.3 Analytical model for charge weld prediction

One of the earliest approaches to analytical modeling of charge weld length was introduced by Valberg [8], who expressed the thickness of the co-extruded layer, t, as a function of a profile-dependent constant, K, the perimeter of the profile, L_p, and the length of the profile measured from the location of the weld plane cusp, l:

$$t = \frac{K}{L_p \cdot l} \tag{2}$$

This formula was based on consideration of the portion of material trapped at die corners between successive billets for simple axisymmetric profiles. During extrusion, this material is gradually pushed out and completely replaced by the new billet. Valberg therefore sought to estimate the thickness of the leftover portion from the previous billet, which progressively decreases as the length of the new extruded billet increases. While providing a simple estimate, the applicability of this model was limited by the coefficient K, which must be calibrated for specific profile types and die configurations and therefore may not be accurate for more complex or multi-port hollow sections typical of industrial production. A subsequent formulation by Saha [34] expressed the charge weld extent, d, as a simple function of the material volume within the die port, $V1$, the material volume within the welding chamber, $V2$, the profile exit area, A_e, and the number of die openings, n:

$$d = \frac{(V1 + V2)}{A_e \cdot n} \tag{3}$$

Jowett et al. [35] introduced a corrective factor by multiplying Eq. (3) by 1.5, improving agreement with experimental measurements. This adjustment accounted for the fact that not all of the port volume contributes to material flow due to the presence of dead metal zones, and that material at the center of the ports moves faster than that adjacent to the walls due to friction. Both factors tend to increase the actual defect length compared to Saha's original prediction, justifying the use of the additional coefficient in Jowett's formula.

The analytical model developed within the present study builds upon the groundwork provided by these works, introducing additional parameters to greatly improve applicability to industrially-relevant die and profile geometries. The geometric parameters presented in Fig. 5 were therefore selected based on industrial experience and previous studies. The objective of the developed model was to introduce penalty coefficients to account for the complexity of the die geometry and consequently correct predictions provided by the Saha model.

In addition to the geometric parameters defined within Saha's formulation in Eq. (3), two local extrusion ratios were calculated to account for the evolution of material flow from die entry to bearing exit. The parameter R_1 was defined as the maximum ratio of the inlet area of an individual feeder to the area feeding the welding chamber as per Eq. (4). The parameter R_2 was defined as the maximum ratio of the area feeding the welding chamber to the exit area of the profile segment associated with that feeder as per Eq. (5). A value of R_1 close to 1 combined with a high value of R_2 therefore

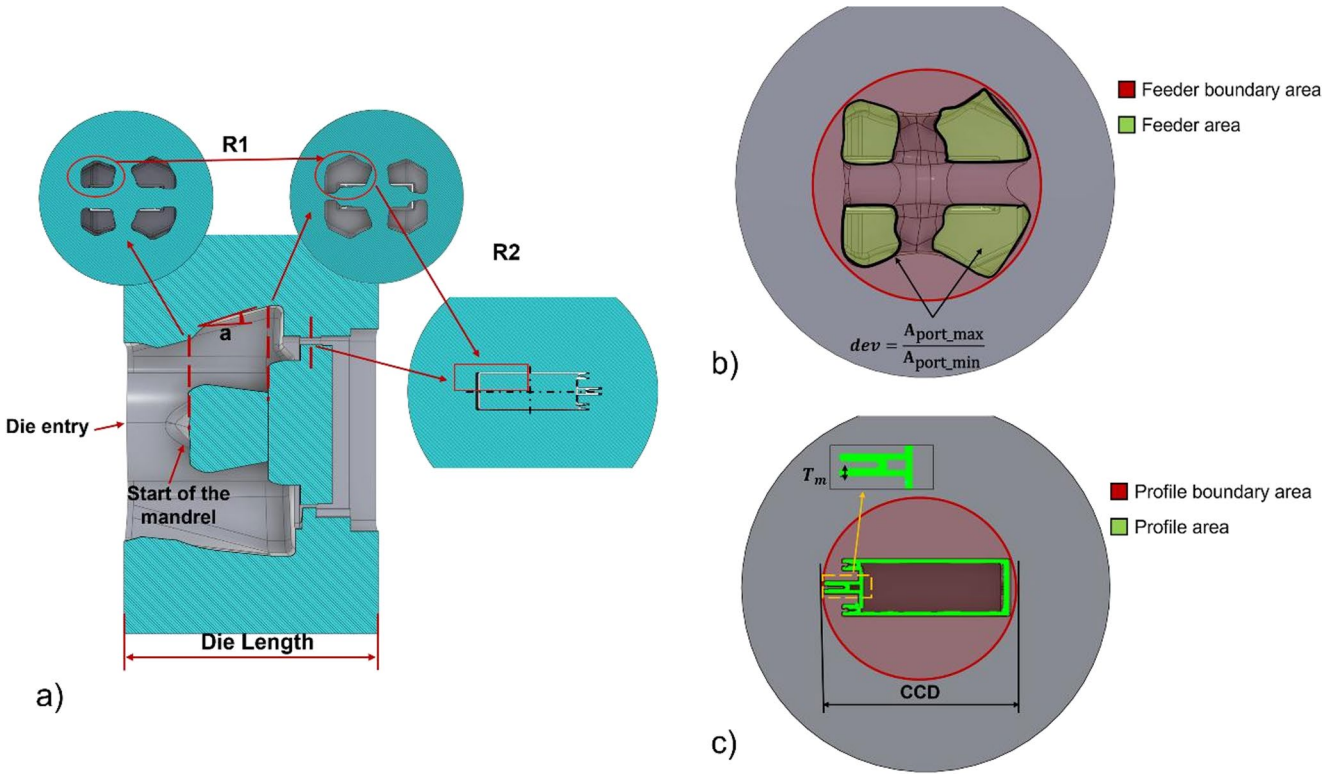

Fig. 5 Geometric parameters used as inputs for the analytical model: **a**) die cross-section; **b**) feeder-related parameters; **c**) profile-related parameters

indicated strong convergence of material flow at the exit; a condition that could potentially promote faster charge weld extinction and therefore decreased scrap length.

The maximum convergence or divergence angle of the feeder chamber, α_{die}, was also considered to account for the effects of flow convergence, as it was expected that divergent flow would increase defect persistence, while convergent flow would accelerate its decay. The diameter of the circumscribed circular area of the profile, *CCD*, and the minimum profile wall thickness, T_m, were accounted for to incorporate the complexity index, C_3 as per Eq. (6), based on the methodology proposed by Qamar [16]. Higher C_3 values, associated with thin sections or details located far from the die axis, were expected to slow down defect extinction and consequently increase the scrap length. Additional significant parameters included the maximum and minimum port areas, A_{port_max} and A_{port_min} respectively, the die length, L_{die}, and the areas circumscribing both the feeders and the exit profile, $A_{cf.}$ and $A_{cp.}$ respectively. The latter two quantities were included to account for the complexity of the die, as small values of effective feeding and exit areas compared to their circumscribed region were considered as indicating higher complexity.

A set of descriptors was calculated based on these quantities with the aim of capturing the combined geometric complexity of the die and extruded profile. Specifically, the deviation parameter *dev*, the novel synthetic complexity index J_m, deviation metrics dev_4 and dev_5, and geometric parameter L_1, were defined as per Eqs. (7)-(11), as well as the parameter C_{d_die} defined as per Eq. (12):

$$R_1 = \frac{A_{billet}}{A_{port\_entrace}} \tag{4}$$

$$R_2 = \frac{A_{port\_exit}}{A_{profile}} \tag{5}$$

$$C_3 = \frac{CCD}{T_m} \tag{6}$$

$$dev = \frac{A_{\mathrm{port\_max}}}{A_{\mathrm{port\_min}}} \tag{7}$$

$$J_m = \frac{\left(\frac{V}{A \cdot n}\right) * dev^{a_1} * \left(1 + a_2 * exp\left(\frac{-a_3 * R_2}{R_1}\right)\right)}{1 \pm sin\alpha} \tag{8}$$

$$dev_4 = \frac{A_{cp}}{A_{profile}} \tag{9}$$

$$dev_5 = \frac{A_{cf}}{A_{feeder}} \tag{10}$$

$$L_1 = \frac{\frac{V}{(A_{feeder})}}{L_{die}} \tag{11}$$

$$C_{d\_die} = 1 + \sin\left(\alpha_{die}\right) \tag{12}$$

where $a_1 \ldots a_3$ are coefficients to be determined based on acquired data. These descriptors were then used as inputs to calculate the predicted charge weld length in the extrusion direction, d_{cw}:

$$d_{cw} = J_m + b_1 \cdot C_3^{b2} + b_3 \cdot Dev_4^{b4} + b_5 \cdot Dev_5^{b6} + b_7 \cdot L_1^{b8} + b_9 \cdot C_{d\_die}^{b10} \tag{13}$$

where $b_1 \ldots b_9$ are coefficients to be determined based on acquired data. Coefficients within the proposed model were obtained via nonlinear regression in MATLAB using the function *nlinfit*. Acquired data (see Sections 2.1 and 2.2) were firstly organized into predictor and response arrays, after which a single function was defined to describe model behavior. The nonlinear regression algorithm within *nlinfit* performed iterative nonlinear least-squares regression based on user-defined initial values with the Levenberg–Marquardt method until obtaining convergence of coefficient estimates. The final set of coefficients obtained with this procedure was subsequently used in the model for further analysis and validation.

3 Results and discussion

3.1 Comparison between FEM simulation and experimental charge welds

Figure 6 presents examples of experimental charge weld evolution for Profile_exp_1 and Profile_exp_3, representing solid and hollow profiles, at three different distances from the stopmark. The presence of new billet material (red region in Fig. 6) initiates at the center of Profile_exp_1, expanding towards the profile boundaries as the distance from the stopmark increases. The threshold for defect extinction (>99% new billet material) was achieved within 500 mm from the stop mark. More complex behavior can instead be observed for Profile_exp_3, with large quantities of old billet material persisting beyond 1100 mm from the stopmark, with gradual expansion of new billet material along the thin central walls and finally along the thicker left-hand wall. In this case, the threshold for defect extinction was achieved within 2500 mm from the stop mark, implying five times the scrap length than for Profile_exp_1. This outcome was due to the high extrusion ration and complex deformation required to achieve Profile_exp_3.

Upon validation of FEM simulations based on the extrusion load and temperature distribution for Profile_exp_1 to Profile_exp_12 (see Section 2.2), a comparison between the real and predicted charge weld length was performed

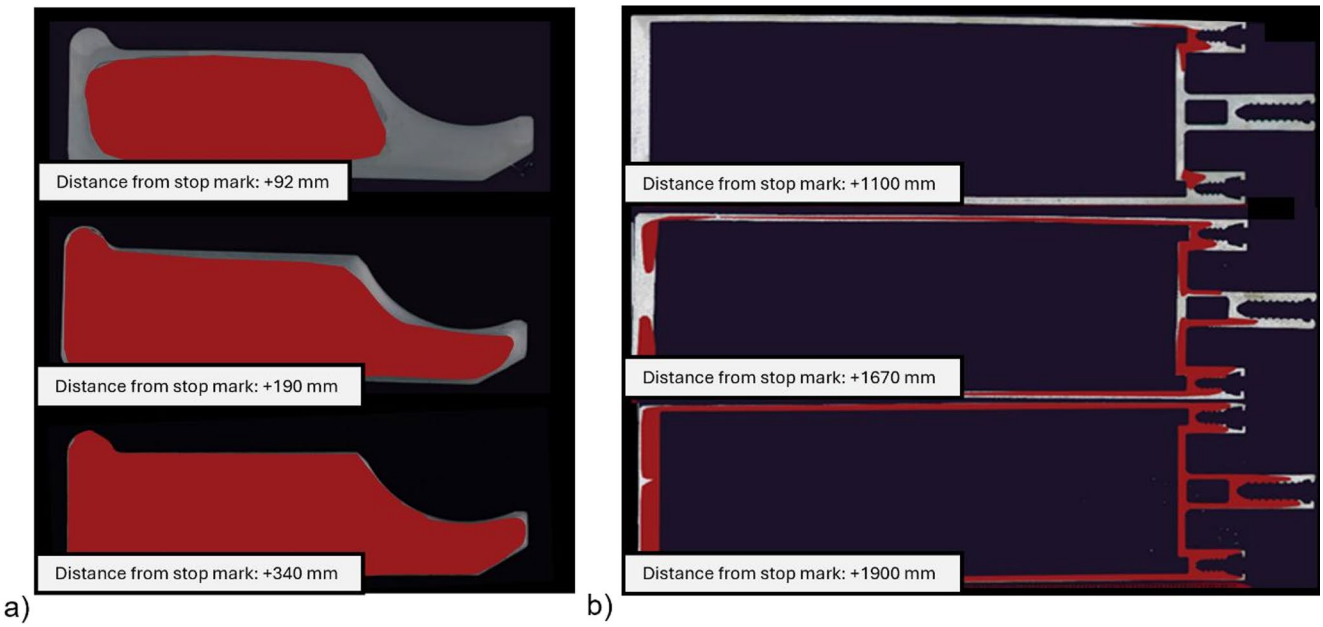

Fig. 6 Example of experimental charge weld evolution at three different distances from stopmark: **a**) Profile_exp_1; **b**) Profile_exp_3. Red: new billet material

for the same profiles. Table 5 and Fig. 7 show that the prediction error was consistently below 10% of the measured value. The mean absolute percentage error (MAPE) was 7.74%, confirming the reliability of the developed FEM model. Figure 8 provides a qualitative representation of selected profiles, showing that the shape of the new billet material within the profile section, highlighted in red within the figure, accurately matches experimental results. These outcomes further validated the FEM model and supported expansion of the dataset through generation of additional numerical results for additional cases, an essential step towards building a sufficiently large dataset for calibrating the analytical model.

Having confirmed agreement between experimental observations and FEM simulations, an additional 84 extruded profiles were simulated via FEM with the aim of compiling a sufficiently large dataset for regression of analytical model coefficients in a robust and representative manner. Additional data were combined with the 12 experimental cases to obtain a final dataset comprising 96 entries. To guarantee statistical representativeness, the dataset was designed to cover a broad range of process parameters, including all die geometry features indicated in Fig. 5, thus allowing the regression model to capture nonlinear dependencies across the full process window.

3.2 Final dataset

Figure 9 presents the occurrence frequency of the main variables within the final dataset. Parts (a)-(i) report the frequency of input variables described in Section 2.3, while part (l) reports the frequency of the measured or simulated charge weld length within the final dataset. Most input quantities exhibit skewed distributions, with higher frequency at lower values. The parameter $V / (A \times h)$, employed to estimate charge weld extent by Saha as per Eq. (3), exhibits a peak at approximately 500 mm (Fig. 9a), with more than 40 occurrences, followed by a sparse distribution up to approximately 4500 mm. This suggests that the majority of cases correspond to relatively low normalized volumes, with only a few cases having higher values.

The deviation factor *dev* is concentrated near 1 (Fig. 9b), with over 70 occurrences falling within the range 1-1.5. Such narrow clustering highlights the fact that most geometries present minimal deviation, with a limited number of cases reaching values above 6. Similarly, the distribution of R_1 (Fig. 9c) exhibits roughly 65 occurrences below 2, with only a small number of points extending up to 12, emphasizing the predominance of low R_1 ratios. Conversely, R_2 exhibits a more dispersed distribution (Fig. 9d), with a range of high values between 4 and 7 and a long tail extending up to values above 30, indicating greater variability of this parameter.

C_3 presents strong skewness (Fig. 9e), with the majority of data below 20 and only a few points exceeding 100. A similar trend can be seen for dev_4 (Fig. 9f), where about 45 cases are concentrated below 5, while sporadic occurrences appear up to 40. The parameter dev_5 maintains a similar shape (Fig. 9g), with the major of values between 1 and 3 and a few scattered up to approximately 11. The distribution

Table 5 Comparison of real (experimental) and predicted (FEM) charge weld length for 12 extruded profiles

Charge weld	Profile_exp_1	Profile_exp_2	Profile_exp_3	Profile_exp_4	Profile_exp_5	Profile_exp_6	Profile_exp_7	Profile_exp_8	Profile_exp_9	Profile_exp_10	Profile_exp_11	Profile_exp_12
Real length [mm]	500	900	2500	2200	2100	910	860	2990	2800	940	1600	2010
Predicted length [mm]	540	850	2300	2400	1980	850	930	2760	3010	1020	1480	2170
Absolute error (%)	8.00%	5.60%	8.00%	9.09%	5.71%	6.59%	8.14%	7.60%	7.50%	8.51%	7.50%	7.96%

of L_1 (Fig. 9h) also follows this pattern, with most data falling below 20 and a sharp drop in frequency for larger values up to approximately 100. In contrast, C_{d_die} (Fig. 9i) exhibits a relatively constant distribution over the range 1.1–1.8, suggesting a more homogeneous distribution.

Finally, the charge weld length (Fig. 9j) exhibits a pronounced peak for weld lengths below 1000 mm. This outcome is consistent with typical industrial practice, as in most extrusion operations the die design is intentionally optimized to minimize scrap and ensure efficient material utilization. As a consequence, short charge welds are systematically pursued during process and die design. This results in a predominance of cases with limited charge weld length, while longer welds represent less frequent or suboptimal configurations. Therefore, the observed statistical distribution is representative of industrially relevant conditions corresponding to low scrap due to charge welds.

3.3 Regression of analytical model coefficients

A non-linear regression was performed to establish a relationship between the geometric variables defined in Eq. (13) and the actual charge weld length defined within the final dataset. Regression coefficients obtained with the MATLAB function *nlinfit* are reported in Table 6.

3.4 Evaluation of analytical model

The developed analytical model was found to exhibit excellent agreement with the actual charge weld length, achieving a MAPE of 8.91% with the final dataset. The model significantly outperformed existing analytical formulations in the literature, including the Saha and Jowett models (see Section 2.3), which yielded values of MAPE of 32.61% and 15.35%, respectively. Figures 10, 11 and 12 compare predicted and actual values of charge weld length for the three models. The model proposed within the present work exhibits tight clustering around the red line in Fig. 10 indicating exact correspondence between predicted and actual values, confirming high accuracy and reliability across the entire final dataset. The blue dashed lines indicate ± 25% error bounds. As can be observed in Fig. 10, all but one prediction falls within this region. In contrast, the number of cases with high error increases significantly when adopting the Saha (Fig. 11) or Jowett (Fig. 12) models. The former largely underestimates the weld length, while the latter larger overestimates the value.

These outcomes are important as they imply that the new analytical model can accurately predict the charge weld length significantly faster than FEM simulations, requiring only the acquisition of geometric parameters relating to the die and extruded profile once model coefficients have

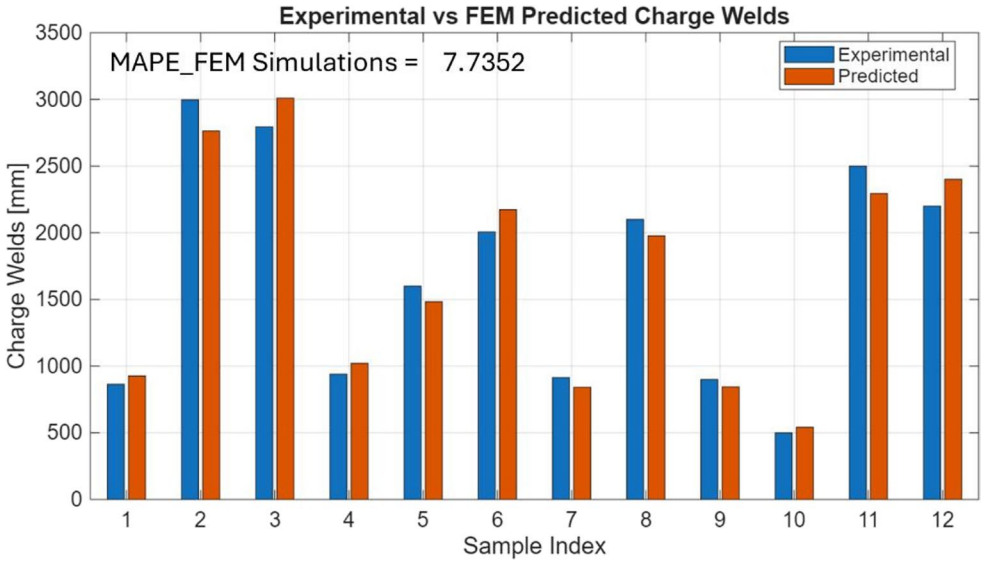

Fig. 7 Comparison of real (experimental) and predicted (FEM) charge weld length for 12 extruded profiles

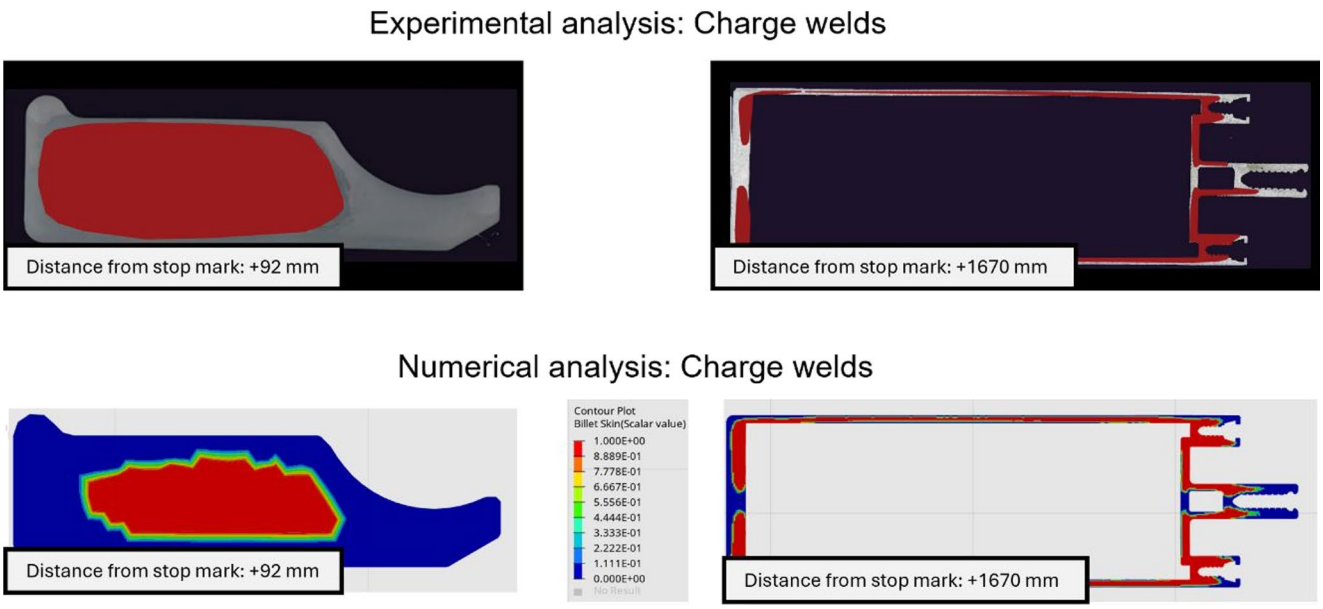

Fig. 8 Qualitative analysis of charge weld evolution in selected profiles at specific distances from the stopmark. Red: new billet material

been determined. Moreover, the formula proposed within this work can also be employed to define an initial set of geometric parameters for die design which, when combined with those provided by other models and operator design experience, can lead to improvements in both the quality and overall efficiency of the die-design process in industrial settings.

4 Conclusion

The present study has proposed a new analytical model for predicting charge weld length in continuous aluminum extrusion using only die and profile geometric parameters. The work was motivated by requirements for faster but reliable alternatives to FEM simulations, which, despite their accuracy, require significant computational resources and are not always practical for industrial die-design workflows. The developed model was shown to provide accurate predictions for complex industrially-relevant profiles by accounting for a wider range of parameters compared to previous analytical approaches, including the inlet area, the area feeding the welding chamber and the exit area, as well as the angle of the feeding chamber, port area and profile wall thickness, amongst others. Model coefficients were determined via non-linear regression based on a combined dataset comprising 12 industrial profiles that were characterized experimentally and an additional 84 profiles that

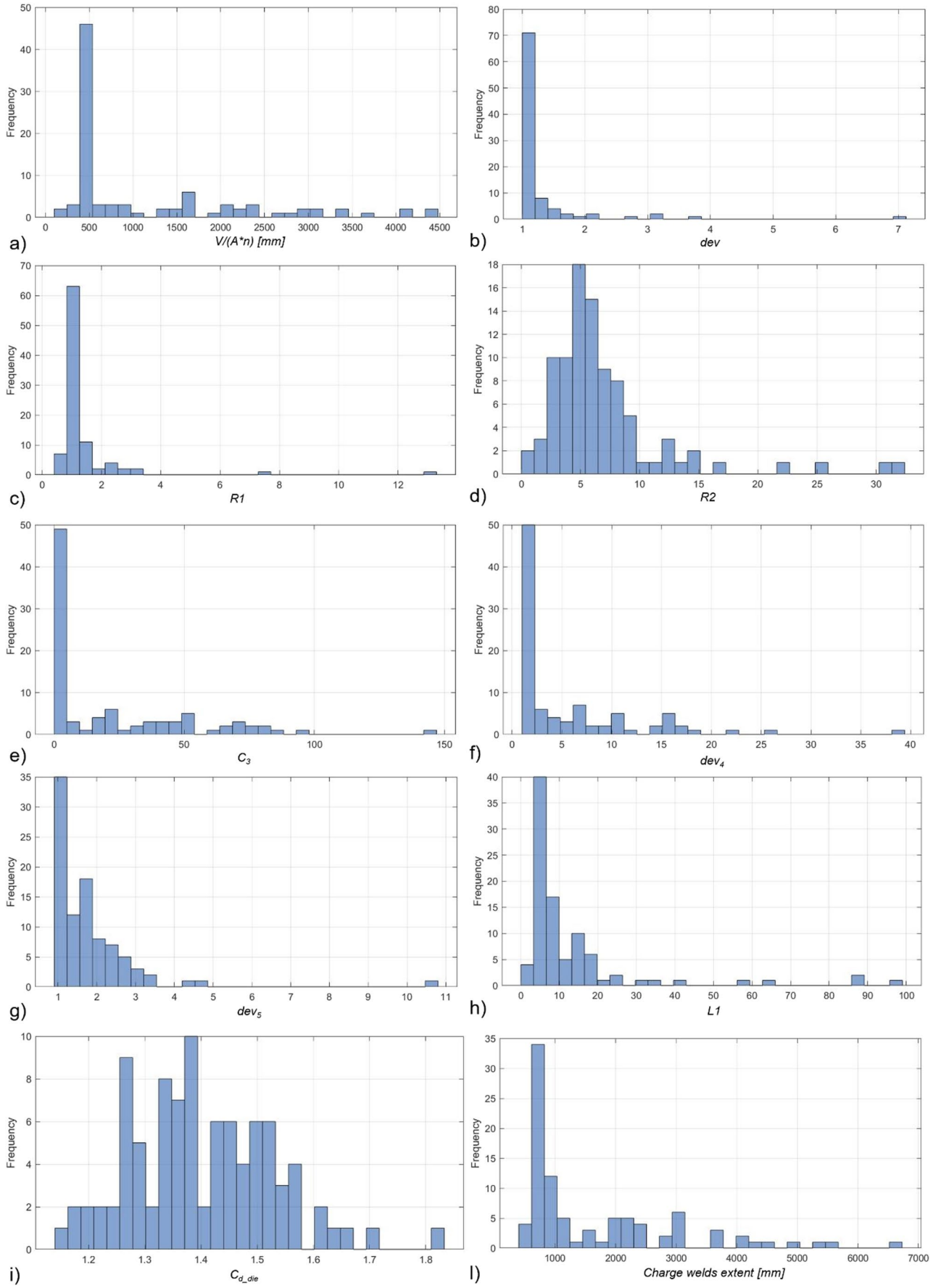
a)
Frequency
V/(A*n) [mm]
b)
Frequency
dev
c)
Frequency
R1
d)
Frequency
R2
e)
Frequency
C_3
f)
Frequency
dev_4
g)
Frequency
dev_5
h)
Frequency
L1
i)
Frequency
C_{d_die}
l)
Frequency
Charge welds extent [mm]

Fig. 9 Frequency of main variables within the final dataset: **a**) V / (A×h); **b**) dev; **c**) R_1; **d**) R_2; **e**) C_3; **f**) dev_4; **g**) dev_5; **h**) L_1; **i**) C_{d_die}; **j**) d_{CW}

were obtained numerically with a FEM simulation developed in Altair HyperXtrude®.

The developed analytical model was found to exhibit excellent agreement with the actual charge weld length, achieving a MAPE of 8.91% compared to 32.61% with the Saha model and 15.35% with the Jowett model. The model was therefore proven capable of accounting for complex relationships between die geometry, flow conditions and charge weld evolution. The formulation presented within this work therefore provides an efficient and accurate tool for estimating charge weld length without the need for time-consuming FEM simulations. Relying solely on readily-available geometric parameters, it offers a practical approach to support both preliminary assessment and iterative optimization during the die-design phase, representing a meaningful advancement toward more predictive, data-driven and time-efficient design strategies in aluminum extrusion. Although the current dataset ensures robust model development within the investigated 6XXX alloys, future work will focus on extending the experimental campaign to additional alloy systems in order to assess the sensitivity of the model to variations in material properties, improve its generalizability and perform a systematic analysis of potential outliers.

Table 6 Analytical model coefficients obtained via nonlinear regression

Model coefficients	Calculated value	Model coefficients	Calculated value
a_1	0.2224	b_5	4.8186
a_2	0.5003	b_6	2.2174
a_3	-0.0044	b_7	-3.8827×10^{-6}
b_1	4.3547	b_8	4.1814
b_2	0.9304	b_9	79.2346
b_3	-45.2850	b_{10}	3.4592
b_4	-2.3049×10^{3}		

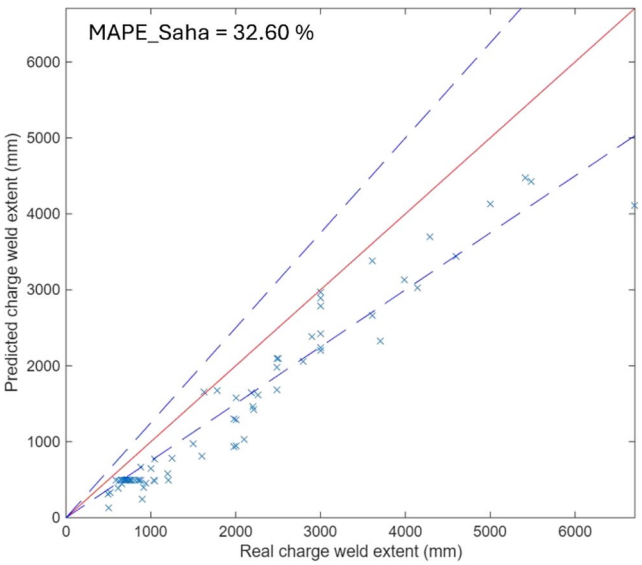

Fig. 11 Comparison of predicted and actual charge weld length with the Saha model (see Section 2.3)

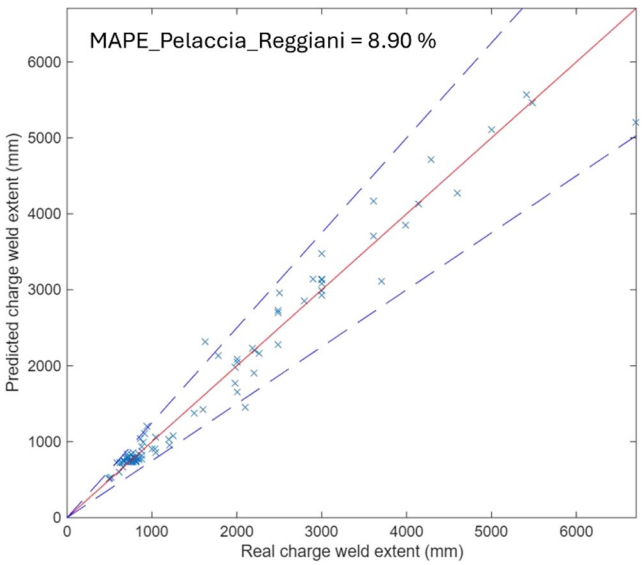

Fig. 10 Comparison of predicted and actual charge weld length with the proposed model (Eq. (12))

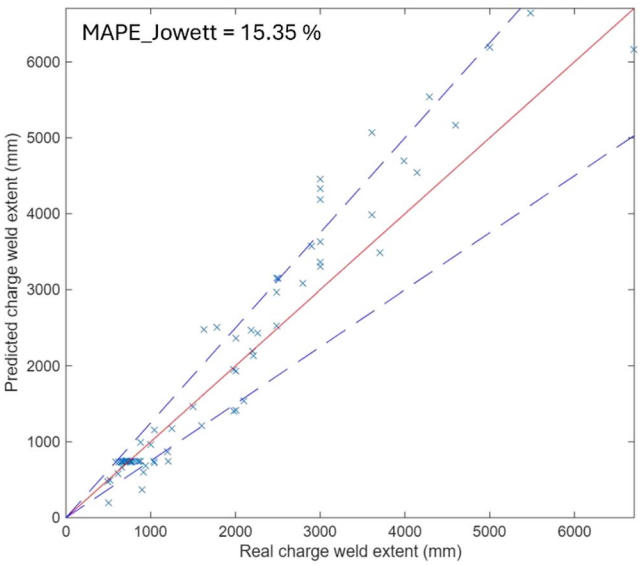

Fig. 12 Comparison of predicted and actual charge weld length with the Jowett model see (Section 2.3)

Acknowledgements This project was supported by PNRR–M4C2INV1.5, NextGenerationEU-Avviso 3277/2021 -ECS_00000033-ECOSISTER-spk 3.

Declarations

Competing interests The authors report there are no competing interests to declare.

References

1. Guo C, Qiao J, Wang W et al (2023) Optimization strategy for the indirect isothermal extrusion of high-strength aluminum alloy based on temporal fusion transformer. Int J Adv Manuf Technol 126:5179–5189. https://doi.org/10.1007/s00170-023-11370-9
2. Zhang G, Zhang C, Zhao J et al (2025) Numerical simulation of the steady-state aluminum alloy extrusion process with finite volume method. Int J Adv Manuf Technol 140:3047–3057. https://doi.org/10.1007/s00170-025-16294-0
3. Zhao H, Sun L, Zhao G et al (2023) Abnormal grain growth behavior and mechanism of 6005A aluminum alloy extrusion profile. J Mater Sci Technol 157:42–59. https://doi.org/10.1016/j.jmst.2023.02.013
4. Negozio M, Donati L, Lutey AHA (2025) Smart extrusion via data-driven prediction of grain size and peripheral coarse grain defect formation. Sci Rep 15:9518. https://doi.org/10.1038/s41598-025-94884-4
5. Zhang Q, Zuo J, Yang C et al (2025) Multi-objective optimization of hot extrusion process parameters for complex cross-section aluminum profiles with high aging response alloys. Int J Adv Manuf Technol 137:1261–1279. https://doi.org/10.1007/s00170-025-15193-8
6. Bingöl S, Ayer Ö, Altinbalik T (2015) Extrusion load prediction of gear-like profile for different die geometries using ANN and FEM with experimental verification. Int J Adv Manuf Technol 76:983–992. https://doi.org/10.1007/s00170-014-6328-z
7. Saha PK (2000) Aluminum extrusion technology. ASM International, Materials Park
8. Valberg H (2002) Extrusion welding in aluminium extrusion. IJMPT 17:497. https://doi.org/10.1504/IJMPT.2002.001317
9. Loukus A, Subhash G, Imaninejad M (2004) Mechanical properties and microstructural characterization of extrusion welds in AA6082-T4. J Mater Sci 39:6561–6569. https://doi.org/10.1023/B:JMSC.0000044896.46771.ba
10. Zhang X, Feng D, Shi X, Liu S (2013) Oxide distribution and microstructure in welding zones from porthole die extrusion. Trans Nonferrous Met Soc China 23:765–772. https://doi.org/10.1016/S1003-6326(13)62527-3
11. den Bakker AJ, Katgerman L, van Zwaag S D (2016) Analysis of the structure and resulting mechanical properties of aluminium extrusions containing a charge weld interface. J Mater Process Technol 229:9–21. https://doi.org/10.1016/j.jmatprotec.2015.09.013
12. Lou S, Wang A, Lu S et al (2019) Tensile property and micro-texture evolution of the charge weld in a billet-to-billet extrusion of AA6061 aluminum profile. Int J Adv Manuf Technol 103:1309–1323. https://doi.org/10.1007/s00170-019-03573-w
13. Yu J, Zhao G, Zhao X et al (2019) Microstructures of longitudinal/transverse welds and back-end defects and their influences on the corrosion resistance and mechanical properties of aluminum alloy extrusion profiles. J Mater Process Technol 267:1–16. https://doi.org/10.1016/j.jmatprotec.2018.12.006
14. Bingöl S, Bozacı A (2015) Experimental and Numerical Study on the Strength of Aluminum Extrusion Welding. Materials 8:4389–4399. https://doi.org/10.3390/ma8074389
15. Zhang C, Dong Y, Wang C et al (2017) Evolution of transverse weld during porthole extrusion of AA7N01 hollow profile. J Mater Process Technol 248:103–114. https://doi.org/10.1016/j.jmatprotec.2017.05.017
16. Qamar SZ, Chekotu JC, Al-Maharbi M, Alam K (2019) Shape Complexity in Metal Extrusion: Definitions, Classification, and Applications. Arab J Sci Eng 44:7371–7384. https://doi.org/10.1007/s13369-019-03886-8
17. Oberhausen GJ, Christopher AAA, Cooper DR (2021) Reducing Aluminum Extrusion Transverse Weld Process Scrap. In: Daehn G, Cao J, Kinsey B et al (eds) Forming the Future. Springer International Publishing, Cham, pp 1003–1019
18. Sariyarlioglu EC, Welo T, Ma J (2024) On the mechanisms of charge weld evolution in aluminum extrusion. J Manuf Process 124:377–384. https://doi.org/10.1016/j.jmapro.2024.06.022
19. Li Q, Harris C, Jolly MR (2003) Finite element modelling simulation of transverse welding phenomenon in aluminium extrusion process. Mater Design 24:493–496. https://doi.org/10.1016/S0261-3069(03)00123-7
20. den Bakker AJ, Werkhoven RJ, van de Nolle R (2013) Influence of die geometry on charge weld evolution. In: ICEB 2013-International Conference on Extrusion and Benchmark 8th-9th October. Dortmund, Germany
21. Reggiani B, Segatori A, Donati L, Tomesani L (2013) Prediction of charge welds in hollow profiles extrusion by FEM simulations and experimental validation. Int J Adv Manuf Technol 69:1855–1872. https://doi.org/10.1007/s00170-013-5143-2
22. Mahmoodkhani Y, Wells MA, Parson N, Poole WJ (2014) Numerical modelling of the material flow during extrusion of aluminium alloys and transverse weld formation. J Mater Process Technol 214:688–700. https://doi.org/10.1016/j.jmatprotec.2013.09.028
23. Mahmoodkhani Y, Wells M, Parson N et al (2014) Modeling the Formation of Transverse Weld during Billet-on-Billet Extrusion. Materials 7:3470–3480. https://doi.org/10.3390/ma7053470
24. Pinter T, Reggiani B, Donati L, Tomesani L (2015) Numerical Assessment of the Influence of Process and Geometric Parameters on Extrusion Welds and Die Deformation after Multiple-cycles. Mater Today: Proc 2:4856–4865. https://doi.org/10.1016/j.matpr.2015.10.034
25. Negozio M, Pelaccia R, Donati L et al (2021) Finite Element Model Prediction of Charge Weld Behaviour in AA6082 and AA6063 Extruded Profiles. J Materi Eng Perform 30:4691–4699. https://doi.org/10.1007/s11665-021-05752-x
26. Di Donato S, Pelaccia R, Negozio M (2024) Phase Field Method for the Assessment of the New-Old Billet Material Interaction during Continuous Extrusion Using COMSOL Multiphysics. J Materi Eng Perform 34:6963–6977. https://doi.org/10.1007/s11665-024-10013-8
27. Di Donato S, Pelaccia R, Negozio M et al (2025) Modeling of charge welds evolution through Cahn-Hilliard equation for interaction between different fluids: experimental-numerical comparison with industrial case studies. Mater Res Proc 54:799–808. https://doi.org/10.21741/9781644903599-86
28. Pelaccia R, Negozio M, Di Donato S et al (2024) Numerical simulation of the extrusion process with different FEM code approaches: analysis of thermal field, profile speed, defects evolution, and microstructure of hollow tubes. Mater Res Proc 41:771–780. https://doi.org/10.21741/9781644903131-85
29. Sariyarlioglu EC, Negozio M, Welo T, Ma J (2024) Charge weld evolution in hollow aluminum extrusion: Experiments and modeling. CIRP J Manufact Sci Technol 49:14–27. https://doi.org/10.1016/j.cirpj.2023.12.007
30. Pinter T, Anotnios T, Reggiani B, Gamberoni A (2016) Charge weld scrap minimization by means of dead metal flow control in die design. In: Proceedings of the Eleventh International Aluminum Extrusion Technology Seminar (ET 2016). Chicago, Illinois, pp 827–845

31. Zhang C, Zhao G, Chen H et al (2012) Numerical simulation and metal flow analysis of hot extrusion process for a complex hollow aluminum profile. Int J Adv Manuf Technol 60:101–110. https://doi.org/10.1007/s00170-011-3609-7
32. Crosio M, Hora D, Becker C, Hora P (2018) Realistic representation and investigation of charge weld evolution during direct porthole die extrusion processes through FE-analysis. 8. https://doi.org/10.3929/ETHZ-B-000300157
33. Qamar Z, Sheikh AK, Arif AFM, Pervez T (2007) Defining Shape Complexity of Extrusion Dies—A Reliabilistic View. Mater Manuf Processes 22:804–810. https://doi.org/10.1080/10426910701446689
34. Saha P (2008) Quality issues of hollow extrusions for aerospace applications. In: Proceedings of the 9th aluminum extrusion technology seminar. Orlando, Florida, pp 441–458
35. Jowett C, Adams J, Daughetee C et al (2008) Scrap allocation. In: Proceedings of the 9th Aluminum Extrusion TechnologySeminar. Orlando, Florida, pp 223–244
36. Parson N, Fourmann J, Beland J (2017) Aluminum extrusions for automotive crash applications. SAE Technical Paper 2017-01-1272. https://doi.org/10.4271/2017-01-1272
37. El Mehtedi M, Musharavati F, Spigarelli S (2014) Modelling of the flow behaviour of wrought aluminium alloys at elevated temperatures by a new constitutive equation. Mater Des (1980–2015) 54:869–873. https://doi.org/10.1016/j.matdes.2013.09.013
38. Negozio M, Donati L, Pelaccia R et al (2023) Experimental analysis and modeling of the recrystallization behaviour of a AA6060 extruded profile. Mater Res Proc 28:477–486. https://doi.org/10.21741/9781644902479-52
39. Negozio M, Segatori A, Pelaccia R et al (2024) Modeling of recrystallization behaviour of AA6xxx aluminum alloy during extrusion process. Trans Nonferrous Met Soc China 34:3170–3184. https://doi.org/10.1016/S1003-6326(24)66600-8
40. Negozio M, Di Donato S, Pelaccia R et al (2025) Impact of die design and bearing geometry on grain size and PCG formation during extrusion of AA6082 aluminum alloy. J Mater Sci Technol 230:80–92. https://doi.org/10.1016/j.jmst.2025.01.017
41. Bajor T, Kawałek A, Berski S et al (2022) Analysis of the Extrusion Process of Aluminium Alloy Profiles. Materials 15:8311. https://doi.org/10.3390/ma15238311